



University
of Glasgow

Dogonchi, A.S., Nayak, M.K., Karimi, N., Chamkha, A. J. and Ganji, D.D. (2020) Numerical simulation of hydrothermal features of Cu-H₂O nanofluid natural convection within a porous annulus considering diverse configurations of heater. *Journal of Thermal Analysis and Calorimetry*, 141, pp. 2109-2125. (doi: [10.1007/s10973-020-09419-y](https://doi.org/10.1007/s10973-020-09419-y))

There may be differences between this version and the published version. You are advised to consult the publisher's version if you wish to cite from it.

<http://eprints.gla.ac.uk/209482/>

Deposited on 5 February 2020

Enlighten – Research publications by members of the University of Glasgow
<http://eprints.gla.ac.uk>

Numerical simulation of hydrothermal features of Cu-H₂O nanofluid natural convection within a porous annulus considering diverse configurations of heater

A.S. Dogonchi^{1*}, M. K. Nayak², N. Karimi³, Ali J. Chamkha^{4,5}, D.D. Ganji⁶

¹Department of Mechanical Engineering, Aliabad Katoul Branch, Islamic Azad University, Aliabad Katoul, Iran.

²Department of Physics, IHSE, Siksha “O” Anusandhan Deemed to be University, Bhubaneswar-751003, Odisha, India

³School of Engineering, University of Glasgow, Glasgow, UK

⁴Mechanical Engineering Department, Prince Sultan Endowment for Energy and Environment, Prince Mohammad Bin Fahd University, Al-Khobar 31952, Saudi Arabia

⁵RAK Research and Innovation Center, American University of Ras Al Khaimah, United Arab Emirates

⁶Mechanical Engineering Department, Babol Noshirvani University of Technology, Babol, Iran

*Corresponding author: E-mail: sattar.dogonchi@yahoo.com

Abstract

The purpose of the current study is to numerically investigate the effects of shape factors of nanoparticles on natural convection in a fluid saturated porous annulus developed between the elliptical cylinder and square enclosure. A numerical method called the control volume-based finite element method (CVFEM) is implemented for solving the governing equations. The modified flow and thermal structures and corresponding heat transfer features are investigated. Numerical outcomes reveal very good grid independency and excellent agreement with the existing studies. The obtained results convey that at a certain aspect ratio, increment of Rayleigh and Darcy numbers significantly augments the heat transfer and average Nusselt number. Further, enhancement of Rayleigh number increases the velocity of nanofluid while that of aspect ratio of the elliptical cylinder shows the opposite trend.

Keywords: Square enclosure; inclined elliptical cylinder; Cu-H₂O nanofluids; diverse configurations of heater; CVFEM.

Nomenclature

(u, v) velocity components in (x, y) directions

ρ density

(ρC_p) heat capacity

μ	dynamic viscosity
β	thermal expansion
k	thermal conductivity
K	permeability parameter
T	temperature
p	pressure
m	shape factor
ω	vorticity
ψ	stream function
α	thermal diffusivity
T_h	temperature at the hot side of the enclosure
T_c	temperature at the cold side of the enclosure
Pr	Prandtl number
Ra	Raleigh number
Da	Darcy number
AR	aspect ratio

Subscripts

f	base fluid
nf	nanofluid
s	solid nanoparticle

1. Introduction

Engineers constantly look for innovative methods to improve heat transfer performance by implementing a wide range of techniques. Natural convection is widely perceived as the ultimate heat transfer process in numerous engineering devices includes enclosures with heat-generating elements. Natural Convection in porous media has attracted intensive attention from

researchers in the view of its relevance in infiltrating molten metal, transport processes, extracting crude oil from oil reservoirs, geothermal operations, chemical reactors, thermal reservoirs, insulating buildings, see for example Nield and Bejan [1], Ingham and Pop [2], Sajid and Ali [3], Guerrero Martinez et al. [4,5]. In particular, the problem of natural convection of nanofluids in porous media has already received considerable attention. Here, we briefly review some of the recent works in this field.

Siavashi et al. [6] have examined the mixed convection within a porous enclosure filled with non-Newtonian nanoliquid. Izadi et al. [7] discussed the impingement of a jet of air, hydrogen and Cu-H₂O nanofluid over a hot surface covered by porous media with non-uniform input jet velocity. They observed that rise in the volume fraction of nanoliquid augmented the heat transfer rate. They also perceived that the utilization of non-uniform impingement jet with diminishing velocity distribution upgrades the thermal performance of the heat sink. Xiong et al. [8] investigated the influences of nanoparticles with diverse shapes on magnetic radiative flow within wavy porous space. In their investigation, roles of magnetic parameter, radiation parameter, nanoparticles' shape and Rayleigh number have been explored. Outputs revealed that applied magnetic field uplifts the temperature distribution and the Nu_{ave} amplifies with Ra and Da numbers as well as nanoparticles' shape, while magnetic field has the opposite impact.

Bozorg et al. [9] carried out a numerical investigation of heat transfer and oil-Al₂O₃ nanoliquid flow inside a parabolic trough solar receiver with internal porous structure. The results displayed that incremented Reynolds number and volume fraction of nanoparticle yielded an augmentation in thermal efficiency, pressure drop and heat transfer coefficient. However, the rise in inlet temperature reduces them. At Re higher than 30×10^4 , concurrent usage of nanoparticles and porous structure with Da = 0.3 augments pressure drops up to 42.5% and 42%, exergetic efficiencies by 7% and 15%, thermal efficiencies up to 8% and 15% and heat transfer coefficients nearly 7%, and 20% for inlet temperature of 500 and 600 K, respectively. Varol et al. [10] scrutinized entropy generation during natural convection inside non-evenly heated porous triangular cavity. Lee et al. [11] studied natural convection inside an annulus among a circular cylinder and enclosure locally heated from the bottom wall. Yoon et al. [12] examined the role of natural convection within a square enclosure considering two cylinders as heater and cooler. Sheremet et al. [13] implemented Tiwari and Das nanofluid model and explored the effects of natural convection inside a square porous cavity. Selimefendigil and Öztop [14] demonstrated the impacts of internal heat generation and inclined magnetic field on natural convection in a flexible sided triangular cavity.

Mun et al. [15] analyzed the effects of vertical and horizontal equal distance of internal hot cylinders on natural convection inside a cold enclosure. Bondareva and Sheremet [16] investigated natural convection melting in a square cavity with a local heater. Rajarathinam and Nithyadevi [17] showed the heat transfer growth of Cu-H₂O nanoliquid in an inclined porous cavity with internal heat generation. Dogonchi and Ganji [18] investigated the impact of Cattaneo-Christov heat flux on magnetic radiative nanoliquid flow and heat transfer among parallel plates. Further, Dogonchi et al. [19] studied the magnetic natural convection of Cu-H₂O nanoliquid in a horizontal semi-cylinder with a local triangular heater. In a separate work, Dogonchi et al. [20] revealed through numerical analysis the influences of natural convection of Cu-H₂O nanoliquid filling triangular enclosure with semicircular bottom wall.

In a numerical study, Nayak [21] worked on magnetic 3D flow and heat transfer analysis of nanofluid by shrinking surface and declared the effect of thermal radiation and viscous dissipation there. The same group of authors [22] discussed natural convection effects on 3D magnetic flow of nanofluid over permeable stretched surface with thermal radiation. Malekpour et al. [23] analyzed the effects of magnetic, natural convection and entropy generation of Cu-H₂O nanoliquid in an I-shape enclosure. Further, Graphene nanoplatelets nanoliquids thermal and hydrodynamic performance on integral fin heat sink (Arshad and Ali [24]), pressure drop and heat transfer in a straight mini-channel heat sink using TiO₂ nanofluid (Arshad and Ali [25]), solar dish assisted S-CO₂ Brayton cycle using nanoliquids flow (Khan et al. [26]) and potential evaluation of ferric oxide and titania nanofluids (Babar and Ali [27]) were carried out. Many other works have been conducted on natural convection within a variety of enclosures containing diverse types of inner bodies of various configurations implementing numerical computations/approaches such as finite volume, finite difference, and finite element method [28-34].

In order to analyze the problems associated with flow through porous media the models such as the Darcy, Forchheimer-extended Darcy, and the Brinkman-extended Darcy models are usually invoked. Choi and Eastman [35] developed nanofluids (nanoscale particles are suspended in a base fluid) which served as the best medium for an effective and efficient convective heat transfer process imparting high-performance energy efficient cooling system needed for many modern applications. According to the thermo-physical features of nanofluids as well as the particle shapes, sizes, stabilities and volume fractions, nanoliquids with superior thermal conductivity (compared to the base fluids) augments its heat transfer characteristics [36]. Further, introduction of porous media upgrades conduction in addition to the existing convection because of the larger surface contact area occupying among porous structure and

working fluid. Consequently, simultaneous application of nanofluids and porous media augments HTR tremendously in comparatively smaller size systems. In this regard, flow through porous media in diverse geometries (Mahdi et al. [37], Kasaeian et al. [38], Torabi et al. [39] and Nayak et al. [40]) and the impacts of porous fins and Cu-H₂O nano-liquid on entropy generation in natural convection have been considered. Also, application of Darcy–Brinkman–Forchheimer model on the porous region and two-phase mixture model for nanofluid (Siavashi et al. [41]) has received some attention. Furthermore, existing studies have considered the use of parallel LBM for investigating the impact of linear temperature distributions of side walls on entropy generation in a porous enclosure loaded with copper-water nanofluid (Ghasemi and Siavashi [42]).

Bararnia et al. [43] examined the thermal and hydrodynamic behaviors during natural convection around a horizontal elliptical cylinder within a cavity for Rayleigh numbers of 10^3 - 10^6 . They revealed that the mean Nu augmented with uplift in the Rayleigh number. Gholamalipour et al. [44] conveyed the influence of eccentricity of heat source inside a porous annulus on the entropy generation and natural convection. Siavashi et al. [45] revealed the behavior of double-pipe heat exchanger using nanoliquid and considering porous media. Asiaei et al. [46] disclosed the multi-layered porous foam impacts on entropy generation and heat transfer of nanoliquid mixed convection within a lid-driven cavity. In a series of numerical investigations, Alizadeh and co-workers examined heat transfer by mixed convection of nanofluids in porous media around cylinders [47-49]. These investigations highlighted the effects of non-cubic porous enclosures and their considerable effects upon the thermal behavior of the system.

The preceding review of literature reveals that a significant effort has been already put on analyzing the influences of several thermal boundary conditions during natural convection in fluid-saturated porous media. However, limited works exist on natural convection in the nanofluid-saturated porous enclosure involving elliptical cylinder as local heaters. It is important to note that local heaters as the heated elements can be readily found in electronic systems. Natural convection inside an annulus between an inclined elliptical cylinder and a square enclosure has been already studied [50]. However, to the best of authors' knowledge, the influences of diverse configurations of the heater and porous medium on heat transfer in such configuration are yet to be explored. The current study aims to fill in this gap by investigating the impacts of different configurations of an elliptical heater and Darcy model associated with different shape factors in natural convection of Cu-H₂O nanoliquid inside an

annulus between an inclined elliptical cylinder and a square enclosure. The influences of pertinent parameters such as aspect ratio, Darcy number, Raleigh number and shape factor of the study on streamlines, isotherms, the local Nusselt number distribution and averaged Nusselt number are explored and discussed.

2. Problem description and the involved fundamental equations

In the current study, natural convection of Cu-H₂O nanoliquid inside a porous annulus among an inclined elliptical cylinder and a square enclosure is analyzed (see Fig. 1). Using the Boussinesq approximation the governing equations can be expressed as [32,33]

$$\frac{\partial u}{\partial x} + \frac{\partial v}{\partial y} = 0 \quad (1)$$

$$u \frac{\partial u}{\partial x} + v \frac{\partial u}{\partial y} = -\frac{1}{\rho_{nf}} \frac{\partial p}{\partial x} + \frac{\mu_{nf}}{\rho_{nf}} \left(\frac{\partial^2 u}{\partial x^2} + \frac{\partial^2 u}{\partial y^2} \right) - \frac{v_{nf}}{K} u \quad (2)$$

$$u \frac{\partial v}{\partial x} + v \frac{\partial v}{\partial y} = -\frac{1}{\rho_{nf}} \frac{\partial p}{\partial y} + \frac{\mu_{nf}}{\rho_{nf}} \left(\frac{\partial^2 v}{\partial x^2} + \frac{\partial^2 v}{\partial y^2} \right) + \beta_{nf} g (T - T_c) - \frac{v_{nf}}{K} v \quad (3)$$

$$u \frac{\partial T}{\partial x} + v \frac{\partial T}{\partial y} = \alpha_{nf} \left(\frac{\partial^2 T}{\partial x^2} + \frac{\partial^2 T}{\partial y^2} \right) \quad (4)$$

Here, u , v , T , K , and p denote the velocity in the x direction, the velocity in the y direction, the temperature, the permeability of the porous medium and the pressure, respectively.

Considering the impact of nanoparticles shape, the ρ_{nf} , $(\rho C_p)_{nf}$, $(\rho\beta)_{nf}$, μ_{nf} , and k_{nf} are defined as follows [33,51,52]

$$\rho_{nf} = (1-\phi)\rho_f + \phi\rho_s \quad (5)$$

$$(\rho C_p)_{nf} = (1-\phi)(\rho C_p)_f + \phi(\rho C_p)_s \quad (6)$$

$$(\rho\beta)_{nf} = (1-\phi)(\rho\beta)_f + \phi(\rho\beta)_s \quad (7)$$

$$\mu_{nf} = \frac{\mu_f}{(1-\phi)^{2.5}} \quad (8)$$

$$\frac{k_{nf}}{k_f} = \frac{(m-1)k_f + k_s + (1-m)\phi(k_f - k_s)}{(m-1)k_f + k_s - \phi(k_s - k_f)} \quad (9)$$

Here, m denotes the shape factor so that its values can be found in Table 1 [32,53]. Moreover, Table 2 [41] portrays the nanoliquid thermo-physical features.

The vorticity (ω) and stream function (ψ) are expressed as follows:

$$v = -\frac{\partial\psi}{\partial x}, \quad u = \frac{\partial\psi}{\partial y}, \quad \omega = -\frac{\partial u}{\partial y} + \frac{\partial v}{\partial x} \quad (10)$$

Considering the following dimensionless variables:

$$X = \frac{x}{L}, \quad Y = \frac{y}{L}, \quad \Omega = \frac{\omega L^2}{\alpha_f}, \quad \Psi = \frac{\psi}{\alpha_f}, \quad U = \frac{uL}{\alpha_f}, \quad V = \frac{vL}{\alpha_f}, \quad \theta = \frac{T - T_c}{T_h - T_c} \quad (11)$$

the governing equations reduce to non-dimensional form:

$$\frac{\partial\Psi}{\partial Y} \frac{\partial\Omega}{\partial X} - \frac{\partial\Psi}{\partial X} \frac{\partial\Omega}{\partial Y} = \frac{\mu_{nf}}{\mu_f} \frac{\rho_f}{\rho_{nf}} \text{Pr} \left(\frac{\partial^2\Omega}{\partial X^2} + \frac{\partial^2\Omega}{\partial Y^2} - \frac{\Omega}{Da} \right) + \frac{\beta_{nf}}{\beta_f} Ra \text{Pr} \frac{\partial\theta}{\partial X} \quad (12)$$

$$\frac{\partial\Psi}{\partial Y} \frac{\partial\theta}{\partial X} - \frac{\partial\Psi}{\partial X} \frac{\partial\theta}{\partial Y} = \frac{\alpha_{nf}}{\alpha_f} \left(\frac{\partial^2\theta}{\partial X^2} + \frac{\partial^2\theta}{\partial Y^2} \right) \quad (13)$$

$$\frac{\partial^2\Psi}{\partial X^2} + \frac{\partial^2\Psi}{\partial Y^2} = -\Omega \quad (14)$$

under the boundary conditions:

$$\begin{aligned} \theta &= 1 && \text{on the inner inclined elliptical wall} \\ \theta &= 0 && \text{on the outer walls} \\ \Psi &= 0 && \text{on the all walls} \end{aligned} \quad (15)$$

where $Da = K/L^2$, $Ra = g\beta_f(T_h - T_c)L^3/\alpha_f\nu_f$ and $\text{Pr} = \nu_f/\alpha_f$ denote the Darcy, Rayleigh number and Prandtl numbers, respectively.

The Local and average Nusselt numbers ($Nu_{loc.}$ and $Nu_{ave.}$) along the cold wall can be defined as:

$$Nu_{loc.} = \frac{k_{nf}}{k_f} \frac{\partial\theta}{\partial n}, \quad Nu_{ave.} = \frac{1}{S} \int_0^S Nu_{loc.} ds \quad (16)$$

where S denotes the length of the cold wall.

3. Numerical solution and validation

The control volume-based finite element method (CVFEM) is utilized to solve the developed governing equations. CVFEM is a hybrid numerical method. In this method the computational domain is discretized with linear-triangular meshes. This method utilizes upwind scheme to discretize the advection term. Finally, the algebraic equations are solved via Gauss-Seidel approach. For more information about CVFEM, one can refer to Refs [54,55]. Validation of the current code is shown in figure 2. It can be deduced that our code has superb potential to solve complex problems. Further, to ensure mesh independency, Nu_{ave} is gained for diverse mesh sizes (see table 3).

4. Results and discussion

In this section, the impact of the embedded parameters including Rayleigh number ($Ra=10^3, 10^4, 10^5$), Darcy number ($Da=0.1, 100, 200$), aspect ratio ($AR=0.3, 0.4, 0.5$), shape factor of nanoparticles ($m=3, 4.8, 5.7$), and the volume fraction of nanofluid (ϕ) on natural convection of Cu-H₂O nanoliquid inside a porous annulus is investigated. The annulus forms between an inclined elliptical cylinder and a square enclosure and the behaviours of pertinent parameters are illustrated in Figs. 3-11. The influence of shape factors of nanoparticles upon the average Nusselt number Nu_{ave} is noted from Table 4. At a certain amount of Ra , increase in m grows Nu_{ave} in the order of nanoparticle types: spherical ($m=3$), cylindrical ($m=4.8$) and platelet ($m=5.7$). At fixed Ra ($Ra=10^3$ or 10^4 or 10^5), we establish a relation between nanoparticle shapes and Nu_{ave} as $(Nu_{ave})_{spherical} < (Nu_{ave})_{cylindrical} < (Nu_{ave})_{platelet}$. This indicates that the minimum heat transfer rate is attained for spherical nanoparticles and maximum heat transfer rate is attained for platelet nanoparticles in nanofluids irrespective of the value of Ra ($Ra=10^3$ or 10^4 or 10^5). Further, increment in Ra grows Nu_{ave} irrespective of the shape of nanoparticles. More elaborately, we ascertain that $(Nu_{ave})_{Ra=10^3} < (Nu_{ave})_{Ra=10^4} < (Nu_{ave})_{Ra=10^5}$ for all spherical, cylindrical and platelet nanoparticles in nanofluids. Regardless of the shape of nanoparticles (spherical, cylindrical and platelet), the Nu_{ave} is minimum at $Ra=10^3$ and maximum at $Ra=10^5$.

4.1 The influences of active parameters on streamlines and isotherms

Fig. 3 illustrates the behaviour of isothermal lines and streamlines for diverse values of Rayleigh number Ra , associated with nanoliquid having volume fraction of 0.02 ($\phi = 2\%$) and spherical nanoparticle ($m = 3$) and aspect ratio $AR = 0.5$. From eq. (12) it is clear that Ra possesses a positive correlation with the strength of streamlines as a result of which increment in Ra yields the characteristic growth of streamlines. This implicates that the impact of convection on the fluid flow and heat transfer upsurges. Further, just outside the outer rigid elliptical wall, the nanofluid gets warmed and progresses upward due to its lower density. However, in the upper layer, nanofluid gets cooled and thus moves downward. Hence, the rotation of the nanofluid is because of the presence of porous medium ($Da = 0.1$). At $Ra = 10^3$, one vertex on the left part of the cavity and two vertices on the right part of the cavity are formed (Fig.3). The flow as well as thermal field exhibits a symmetric pattern near the vertical centerline inside the cavity.

When Ra grows, i.e. at $Ra = 10^4$, the vertices on both parts of the cavity expand. With further increment in Ra , i.e. at $Ra = 10^5$, vertex on the left part of the cavity expands further, while two vertices on the right part of the cavity merge into a bigger vertex. Therefore, at low value of $Da = 0.1$, the conduction dominated flow and heat transfer phenomenon preponderates even for higher to $Ra = 10^5$. The values of ψ inside the enclosure are seen to be lower at low values of Da regardless of Ra implicating decay of the flow rate. This is because at low values of Da the fluid flow is constrained by the prevailing loosely inter-connected voids in the medium. However, the value of ψ is greater adjacent to the vertical walls for higher Ra compared to the case for low Ra since the buoyancy induced flow augments owing to higher Ra and is limited to the walls because of low Da . At higher Da (e.g. $Da = 200$) vertices on the left as well as the right part of the cavity expand with increment in Ra . However, the expansion is less compared to the case with $Da = 0.1$ (Fig. 3). At lower $Ra = 10^3$, the fluid flow is induced by the weak buoyant force represented by a small magnitude of dimensionless stream function. When the ellipse is at an oblique position in the middle of the annulus, CCW and CW rotations are developed on the left and right directions of hot ellipse, respectively. Further, the velocity of nanofluid is higher on the left side compared to that on right side. This is due to the free motion of the nanofluid at the left side of the ellipse. With the increment of velocity of nanoliquid and Ra , convection will be the major contributor to the resulting heat transfer. The stream lines become denser at the upper layer and adjacent to the top wall.

The same trend is envisaged in the figure 3 with increment of Da ($Da = 200$). It should be noted that in consideration of eq. (3), the resistive force due to the existence of porous medium resulted in reduction of flow velocity. Further, for $Ra = 10^3$, the growth of Da ($Da = 200$) and the corresponding diminutive velocity causes heat transfer chiefly through conduction. In addition, the contours of dimensionless stream-functions (as seen in the figure) at $Ra = 10^3$ and $Da = 200$, will be elliptical lines parallel to the main rigid body. At higher values of Ra , the magnitude of ψ upsurges implying higher velocity. At higher Ra , the isothermal lines become less dense associated with incremented Da as seen in the region of the cavity concern (see Fig 3). Growth of Ra enables isotherm contours to move to the top layers of nanofluid. With the growth of Ra and velocity and the corresponding enhanced convection part, isothermal lines rotate towards the region above the cavity.

Fig. 4 depicts the distribution of streamlines and isotherms for diverse aspect ratios of the elliptical heater at lower $Ra = 10^3$. In other words, alteration in aspect ratio of elliptical heater has a notable impact on the heat transfer features at the enclosure walls and the cylinder surfaces. Figure 4 shows that the streamlines and parallel isotherms spanning the entire cavity exhibit a symmetric pattern about the longer diameter of the ellipse. Such streamline distribution is featured by two vertices which are developed on the right and left portions of the cavity. As the aspect ratio of the elliptical heater rises ($AR = 0.3$ to $AR = 0.4$), the $|\psi_{\max}|$ decreases from 8.62994 to 7.46634 indicating the diminution of the velocity of nanofluid. With further increase of aspect ratio (i.e., $AR = 0.4$ to $AR = 0.5$), the intensity of streamlines $|\psi_{\max}|$ decreases from 7.46634 to 6.20732, imparting further decline of the nanofluid velocity. Moreover, with increase in aspect ratio AR isotherm lines become denser and get closer to each other as observed in the cavity region. This can be explained by noting that the space amongst the top wall of the cavity and the elliptical heater diminishes (Fig. 4). From Fig.4 it is also seen that at $Ra = 10^3$, with increment in AR (from $AR = 0.3$ to $AR = 0.4$) vertex on the left part of the enclosure shrinks while the vertex on the right part remains unchanged. With further increase in AR (e.g. at higher $AR = 0.5$) the vertex on the left part shrinks while that on the right part segregate into different vertices of different sizes.

At higher Ra , i.e. at $Ra = 10^4$, augmentation of AR enables the flow and thermal structures to follow the same trend as the case with lower Ra ($Ra = 10^3$) (see Fig.5). The decay of streamlines is inferred from $|\psi_{\max}|$ values as 27.8342, 27.4855 and 26.1772. Further,

isotherms become less dense due to space reduction with gradual increment of AR . However, at larger value of $Ra = 10^4$, isotherms in the form of larger contours rotate towards the region above the cavity in the presence of porous medium. Also, at fixed AR , for instance at $AR = 0.3$, increment in Ra ($Ra = 10^3$ to $Ra = 10^4$) strengthens the stream function ($|\psi_{\max}| = 8.62994$ to $|\psi_{\max}| = 27.8342$) indicating enhancement of velocity of nanofluid. At higher Ra , i.e., $Ra = 10^4$, increment of AR leads to the shrinkage of the vertex on the left part of the enclosure while that on the right part increases at $AR = 0.4$ and decreases at $AR = 0.5$. With further increase in Ra , i.e. at higher $Ra = 10^5$, the symmetric pattern of streamlines seem to augment at a greater magnitude (i.e., $|\psi_{\max}| = 27.8342$ to $|\psi_{\max}| = 72.5451$) indicating further enhancement of velocity of nanofluid. Also, isotherms uplift in the shape of greater symmetric contours due to increment in Ra (Fig.6). Here the resistive force due to the prevailing porous medium, considering the convection term, leads to symmetric isotherm contours.

With augmented Ra , i.e., at $Ra = 10^5$, increment in aspect ratio AR results in the decline of stream function. The decremented value of $|\psi_{\max}|$ are found to be 72.5451, 61.2719, 57.1238. This means that the velocity of nanofluid gets undermined. Further, at higher $Ra = 10^5$, increase in AR leads to an ascending trend of isothermal lines in the form of asymmetric closed contours since the impact of convection ascends (Fig.6). It is interesting to note here that as Ra grows, isotherms in the upper surface of the elliptical heater have been concentrated less intensely compared to those in the bottom portion of the elliptical heater. This is because the gap among the upper surface of the elliptical heater and the upper wall of the cavity where the convective heat transfer enrooted upsurges. At higher $Ra = 10^5$, increase in AR leads to expansion of vertex on the left part of the cavity while the vertex on the right part shrinks.

4.2 The influences of active parameters on Nusselt number

Fig. 7 demonstrates Nu_{loc} profiles for diverse amounts of Ra ($Ra = 10^3, 10^4, 10^5$) and Da ($Da = 0.1, 100$) for aspect ratios $AR = 0.3, 0.4, 0.5$ associated with spherical nanoparticles. To analyze isothermal lines, we should investigate the shapes linked to Nu_{loc} . We start the analysis of Nu at $Da = 0.1$ and $Ra = 10^3$. Invoking the isothermal lines illustrated in Fig.3 at midpoint of the right wall ($s = 0$), the upward movement causes the temperature gradient to fall and finally becomes insignificant at the top corner. Hence, Nu diminishes and finally vanishes at $s = 0.125$ (the top corner). When isotherms rout the top wall and progress towards the left part

of the enclosure, they coalesce and become denser. Consequently, the temperature gradient and therefore the Nusselt number upsurge.

When we progress from the zone above the left outer wall to the bottom, first isotherm contours become denser indicating augmentation of Nusselt number and gradient. Near the midpoint of the wall, temperature gradient as well as Nusselt number decline. After overcoming the midpoint and going downwards, isotherm contours become denser another time and Nusselt number augments. At the end of the left wall, Nusselt number becomes zero, considering temperature gradient and zero velocity of fluid. Clearly, at the starting of lower outer wall, isotherm contours become denser, and thus, Nusselt number uplifts, but next, they acquire some distance and Nusselt number belittles and vanishes another time, at the bottom and right corners.

Temperature gradient uplifts from the lower corner to the middle part of the right outer wall, and so Nusselt number enhances. We now consider isotherm contours of fig. 3 when $Ra = 10^4$. In this case, Nu and temperature gradient find ascending trend while progressing from the center of right outer wall to the upper corner, where Nu and gradient experience a significant decay. Highly dense isotherm contours at the upper outer wall attain the utmost value at the center of the wall leading to the utmost Nu at the center of the top wall. The upper left corner finds the descending trend of Nu due to fall in temperature gradient. While progressing from the top of left outer wall towards bottom of it, initially temperature gradient and then Nusselt attains a very high value. Later on, Nu decreases gradually and finally becomes zero in downward movement to the lower left corner. As Ra augments, isotherm contours progress towards the upper segment, insignificant temperature gradient and least Nu have been recorded at the lower wall for $Ra = 10^4$. Further, Nu attains an ascending trend following upward motion from the bottom to the center segment of the right wall. Similar trend is visualized for Nusselt number at $Da = 0.1$ and $Ra = 10^5$, but extremely high value is attained for temperature gradient at the upper outer wall near the midpoint and afterwards it decays rapidly. This is the basic cause for the conical shape of Nu at the upper wall. As analyzed earlier, temperature gradient falls more significantly and attains zero value at the lower cold wall for $Ra = 10^5$ where isotherm contours progress towards the zone above the enclosure.

We now analyze Nu for $Da = 100$ and $Ra = 10^3$. Consider the isothermal lines of Fig. 3 associated with $Da = 100$ and $Ra = 10^3$ where the isotherm contours at the center of the enclosure is denser than those of other zones and accordingly $(Nu)_{\max}$ is attained nearly at the

middle of it. Further, the Lorentz force associated with the low velocity and convection term is responsible for the symmetry of isotherm contours thereby representing similar trends at the walls. When $Da = 100$ and $Ra = 10^3$, the number of isotherm contours increases at the top wall and becomes maximum at the middle of this wall. The shape of isothermal lines is parabolic at the left wall and within the top zone. Such lines contrast each other at the two sides of centre. Thus, Nu_{loc} possesses two relative utmost points at the left wall. Isotherm contours and accordingly the trend of Nusselt is appreciable for $Da = 100$ and $Ra = 10^5$.

Having a close look at all parts of Fig. 7, considering the density of isotherm contours at the top outer wall, we observe that local $(Nu)_{max}$ is attained at the upper wall. This density gets augmented due to increment in Ra ($Ra = 10^3, 10^4, 10^5$) thereby Nu upsurges at the top outer wall. On the other hand, isotherm contours progress to the zone above the enclosure thereby declining Nusselt at the lower outer wall. Because of increment in AR , Nu upsurges in the range $0 \leq s \leq 0.025$. Here, Nu increases sharply and attains $(Nu)_{max}$ at $s = 0.25$. In this case, the thermal gradient over the bottom surface of elliptical cylinder augments relatively. With increment in AR , Nu decreases in $0.125 \leq s \leq 0.375$. Further, Nu decreases in $0.375 \leq s \leq 0.625$ compared to that in $0.125 \leq s \leq 0.375$. When $0.375 \leq s \leq 0.625$, Nu escalates with increment in AR . Also, Nu value decreases in $0.625 \leq s \leq 0.875$ compared to its value in $0.375 \leq s \leq 0.625$ but with the same increasing trend of Nu is due to increment in AR . Under this situation, the distance between the bottom wall of cavity and elliptical cylinder diminishes.

It is essential to note that Nu value again rises suddenly in $0.875 \leq s \leq 1$ compared to the previous range $0.625 \leq s \leq 0.875$. At $Ra = 10^3$, increment in Da ($Da = 0.1$ to $Da = 100$), Nu value enhances and the maximum augmentation of HTR is accomplished. When Ra increases ($Ra = 10^3$ to $Ra = 10^4$), heat transfer has been drastically reduced in the range $0.375 \leq s \leq 0.625$, $0.625 \leq s \leq 0.875$ and $0.875 \leq s \leq 1$. This is the influence of increment in Ra . Such influence remains unchanged when $Da = 100$. Increment in AR ($AR = 0.3, 0.4, 0.5$) uplifts heat transfer, but in different magnitudes over different intervals of s . Also, when Da goes up ($Da = 0.1$ to $Da = 100$), at $Ra = 10^4$, heat transfer rate gets slightly augmented in $0.125 \leq s \leq 0.375$ and remains the same over other intervals. When Ra further increases ($Ra = 10^4$ to 10^5), Nu value augments except for the interval $0.625 \leq s \leq 0.875$ where

it declines in both cases of $Da = 0.1$ and $Da = 100$ due to conduction dominated flow. However, at $Ra = 10^5$, increase in Da ($Da = 0.1$ to $Da = 100$) uplifts Nu value in the range of $0.125 \leq s \leq 0.375$ and maintains the same Nu value otherwise.

Fig. 8 shows the average Nu for different amounts of Ra , Da and ϕ when $AR = 0.3$ and $m = 3$. It is visualized from the figure that at a certain amount of Ra , increment in ϕ leads to uplift in the average Nu . Also, at fixed amount of ϕ , increment in Ra causes the average Nu to grow. Further, at fixed value of Ra , rise in Da enhances average Nu . Similar trend of average Nu is envisaged at fixed Da with increasing values of ϕ . Lastly, at fixed ϕ , increment in Da cause the average Nu to grow. At a certain amount of Da , rise in ϕ yields in augmentation of average Nu . Nu_{ave} for various values of Ra, Da and ϕ when $AR = 0.4$ and $m = 3$ is shown in Fig.9. It is seen that at certain value of Ra , increment in ϕ and Da leads to the growth of average Nu . Also, at certain value of ϕ , increment in Da shows the same trend. At fixed ϕ or Da , increment in Ra leads to the uplift of Nu_{ave} . Further, at a given Da rise in ϕ causes an escalation of Nu_{ave} . Fig. 10 conveys Nu_{ave} for diverse values of Ra, Da and ϕ when $AR = 0.3$ and $m = 3$. It is obvious that at fixed Ra , increment in ϕ and Da augments the value of Nu_{ave} . Furthermore, for certain values of ϕ , increment in Da produces the growth of Nu_{ave} . Taking into account the graphs of Figs. 8, 9 and 10, for each value of Ra, Da and ϕ , Nu_{ave} can be determined by interpolation.

Fig.11 reveals the impact of porous medium on the heat transfer in terms of Nu_{ave} for different aspect ratios ($AR = 0.3, 0.4, 0.5$) against different Ra for $Da = 0.1$ and $Da = 100$ separately. At a specified value of Ra , increment in AR leads to growth of Nu_{ave} irrespective of Da ($Da = 0.1$ or $Da = 100$). Same ascending trend of Nu_{ave} is caused by the growth of Da at certain Ra . The maximum rate of heat transfer in nanoliquid is $(Nu_{ave})_{max} = 2.6$ for spherical nanoparticles ($m = 3$) for both $Da = 0.1$ and $Da = 100$.

Finally, we acquire the correlation for the Nu_{ave} in terms of effective parameters of the current work which is expressed as follows:

for AR=0.3:

$$\begin{aligned}
 Nu_{ave.} = & 0.67678 + 3.30939 \times 10^{-5} \times Ra + 1.84706 \times \phi \\
 & + 1.40217 \times 10^{-4} \times Da + 2.79088 \times 10^{-5} \times Ra \times \phi \\
 & - 1.64068 \times 10^{-12} \times Ra \times Da + 6.98334 \times 10^{-7} \times \phi \times Da \\
 & - 1.77797 \times 10^{-10} \times Ra^2 + 49.90877 \times \phi^2 - 7.65815 \times 10^{-8} \times Da^2
 \end{aligned}$$

for AR=0.4:

$$\begin{aligned}
 Nu_{ave.} = & 0.73309 + 3.42963 \times 10^{-5} \times Ra + 1.84079 \times \phi \\
 & + 9.96791 \times 10^{-5} \times Da + 3.19377 \times 10^{-5} \times Ra \times \phi \\
 & - 2.23453 \times 10^{-12} \times Ra \times Da + 1.55217 \times 10^{-6} \times \phi \times Da \\
 & - 1.88184 \times 10^{-10} \times Ra^2 + 57.63472 \times \phi^2 + 1.39199 \times 10^{-7} \times Da^2
 \end{aligned}$$

for AR=0.5:

$$\begin{aligned}
 Nu_{ave.} = & 0.80782 + 3.38089 \times 10^{-5} \times Ra + 2.37374 \times \phi \\
 & + 2.13760 \times 10^{-4} \times Da + 3.51642 \times 10^{-5} \times Ra \times \phi \\
 & - 2.82431 \times 10^{-12} \times Ra \times Da + 1.73253 \times 10^{-6} \times \phi \times Da \\
 & - 1.83391 \times 10^{-10} \times Ra^2 + 48.32723 \times \phi^2 - 3.93329 \times 10^{-7} \times Da^2
 \end{aligned}$$

The R-Squared for these correlations are equal 0.9635, 0.9573 and 0.9655, respectively. It is worth mentioning that Response Surface Method (RSM) has been applied for extraction of correlation's average Nusselt number. The connection between a response variable and independent variables can be recognized by RSM. Further, it can be used as a tool to lessen the number of experiments which causes both time and costs to reduce [56-58].

4. Conclusion

In this analysis, natural convection of Cu-H₂O nanoliquid in a porous annulus between an inclined elliptical cylinder and a square enclosure was investigated. The main concluding remarks of the current study are as follows:

- At certain aspect ratio AR, increment in Rayleigh number Ra augments the stream functions thereby yielding greater velocity of nanofluids.
- As the AR of the elliptical cylinder grows, $|\psi_{max}|$ decays indicating the diminution of the velocity of the nanofluid.

- For certain volume fraction ϕ or Darcy number Da , rise in Ra leads to the uplift of average Nu while at certain Ra , increment in ϕ and Da resulted in the growth of average Nu .
- At certain Ra , larger AR leads to augmentation of Nu_{ave} and therefore uplifts heat transfer irrespective of Da .
- At given Da , rise in ϕ upsurges Nu_{ave} .

References

- [1] D.A. Nield, A. Bejan, *Convection in Porous Media*, Springer-Verlag, New York, 1053-1999.
- [2] D.B. Ingham, I. Pop (Eds.), *Transport phenomena in porous media*, Pergamon, Oxford, 1998, vol. II 2000, vol. III 2005.
- [3] M. U. Sajid, H. M. Ali, Recent advances in application of nanofluids in heat transfer devices: A critical review, *Renew. Sustain. Energy Rev.* 103 (2019) 556-592.
- [4] F. Guerrero Martinez, P. Younger, N. Karimi, S. Kyriakis, 2017 “Three-dimensional numerical simulations of free convection in a layered porous enclosure”, *International Journal of Heat and Mass Transfer*, 106, 1005-1013. DOI [dx.doi.org/10.1016/j.ijheatmasstransfer.2016.10.072](https://doi.org/10.1016/j.ijheatmasstransfer.2016.10.072)
- [5] F. Guerrero Martinez, P. Younger, N. Karimi, 2016 “Three-dimensional numerical model of free convection in sloping porous enclosures”, *International Journal of Heat and Mass Transfer*, 98, 257-267, Doi: [10.1016/j.ijheatmasstransfer.2016.03.029](https://doi.org/10.1016/j.ijheatmasstransfer.2016.03.029).
- [6] M. Siavashi, K. Karimi, Qingang Xiong, M. H. Doranehgard, Numerical analysis of mixed convection of two-phase non-Newtonian nanofluid flow inside a partially porous enclosure with a rotating cylinder, *J. Therm. Anal. Cal.* 137 (2019) 267-287.
- [7] A. Izadi, M. Siavashi, Q. Xiong, Impingement jet hydrogen, air and Cu-H₂O nanofluid cooling of a hot surface covered by porous media with non-uniform input jet velocity, *Int. J. Hydro. Energy* 44 (2019) 15933-15948.
- [8] Q. Xiong, E. Abohamzeh, J. A. Ali, S. M. Hamad, I. Tlili, A. Shafee, H. Habibeh, T. K. Nguyen, Influences of nanoparticles with various shapes on MHD flow inside wavy porous space in appearance of radiation, *J. Mol. Liq.* 292 (2019) 111386.
- [9] M. V. Bozorg, M. H. Doranehgard, K. Hong, Q. Xiong, CFD study of heat transfer and fluid flow in a parabolic trough solar receiver with internal annular porous structure and synthetic oil–Al₂O₃ nanofluid, *Renewable Energy*, 145 (2020) 2598-2614.
- [10] Y. Varol, H.F. Oztop, I. Pop, Entropy generation due to natural convection in non-uniformly heated porous isosceles triangular enclosures at different positions, *Int. J. Heat Mass Transf.* 52 (5–6) (2009) 1193–1205.
- [11] H.J. Lee, J.H. Doo, M.Y. Ha, H.S. Yoon, Effects of thermal boundary conditions on natural convection in a square enclosure with an inner circular cylinder locally heated from the bottom wall, *Int. J. Heat Mass Transf.* 65 (2013) 435–450.
- [12] H.S. Yoon, Y.G. Park, J.H. Jung, Natural convection in a square enclosure with differentially heated two horizontal cylinders, *Numer. Heat Transf.* 65 (2014) 302–326.

- [13] M.A. Sheremet, I. Pop, R. Nazar, Natural convection in a square cavity filled with a porous medium saturated with a nanofluid using the thermal non equilibrium model with a Tiwari and Das nanofluid model, *Int. J. Mech. Sci.* 100 (2015) 312–321.
- [14] F. Selimefendigil, H.F. Öztop, Natural convection in a flexible sided triangular cavity with internal heat generation under the effect of inclined magnetic field, *J. Magn. Magn. Mater.* 417 (2016) 327–337.
- [15] G.S. Mun, Y.G. Park, H.S. Yoon, M. Kim, M.Y. Ha, Natural convection in a cold enclosure with four hot inner cylinders based on diamond arrays (Part-I: Effect of horizontal and vertical equal distance of inner cylinders), *Int. J. Heat Mass Transf.* 111 (2017) 755–770.
- [16] N.S. Bondareva, M.A. Sheremet, Flow and heat transfer evolution of PCM due to natural convection melting in a square cavity with a local heater, *Int. J. Mech. Sci.* 134 (2017) 610–619.
- [17] M. Rajarathinam, N. Nithyadevi, Heat transfer enhancement of Cu-water nanofluid in an inclined porous cavity with internal heat generation, *Therm. Sci. Eng. Prog.* 4 (2017) 35–44.
- [18] A.S. Dogonchi and D.D. Ganji, Impact of Cattaneo-Christov heat flux on MHD nanofluid flow and heat transfer between parallel plates considering thermal radiation effect, *Journal of the Taiwan Institute of Chemical Engineers*, 80(2017)52-63.
- [19] A.S. Dogonchi, M. A. Sheremet, I. Pop, D. D. Ganji, MHD natural convection of Cu/H₂O nanofluid in a horizontal semi cylinder with a local triangular heater. *Int. J. Numer.Methods Heat Fluid Flow* **28**, 2979–2996 (2018).
- [20] A.S. Dogonchi, M. A. Ismael, A. J. Chamkha, D. D. Ganji, Numerical analysis of natural convection of Cu-water nanofluid filling triangular cavity with semicircular bottom wall. *J. Therm. Anal. Calorim.* **135**, 3485–3497 (2019).
- [21] M. K. Nayak, MHD 3D flow and heat transfer analysis of nanofluid by shrinking surface inspired by thermal radiation and viscous dissipation, *Int. J. Mech. Sci.* 125 (2017) 185-193.
- [22] M. K. Nayak, N.S. Akbar, V.S. Pandey, Z.H. Khan, D. Tripathi, 3D free convective MHD flow of nanofluid over permeable linear stretching sheet with thermal radiation, *Powder Technol.* 315 (2017) 205-215.

- [23] A. Malekpour, N. Karimi, A. Mehdizadeh, Magnetohydrodynamics, natural convection and entropy generation of CuO-water nanofluid in an I-shape enclosure, *Journal of Thermal Science and Engineering Applications* 10 (2018) doi:10.1115/1.4041267.
- [24] W. Arshad, H. M. Ali, Graphene nanoplatelets nanofluids thermal and hydrodynamic performance on integral fin heat sink, *Int. J. Heat Mass Transf.*, 107 (2017) 995-1001.
- [25] W. Arshad, H. M. Ali, Experimental investigation of heat transfer and pressure drop in a straight minichannel heat sink using TiO_2 nanofluid, *Int. J. Heat Mass Transf.*, 110 (2017) 248-256.
- [26] M. S. Khan, M. A. Hafiz, M. Ali, K. P. Amber, M. A. Bashir, S. Javed, Comparative performance assessment of solar dish assisted s-CO₂ Brayton cycle using nanofluids, *Appl. Therm. Eng.*, 148 (2019) 295-306.
- [27] H. Babar, H. M. Ali, Airfoil shaped pin-fin heat sink: Potential evaluation of ferric oxide and titania nanofluids, *Energy. Conv. Manag.* 202 (2019) 112194.
- [28] K. Ghasemi, M. Siavashi, MHD nanofluid free convection and entropy generation in porous enclosures with different conductivity ratios, *Journal of Magnetism and Magnetic Materials* 442, 2017, 474-490.
- [29] M. Siavashi, A. Rostami, Two-phase simulation of non-Newtonian nanofluid natural convection in a circular annulus partially or completely filled with porous media, *International Journal of Mechanical Sciences* 133, 2017, 689-703.
- [30] M.H. Toosi, M. Siavashi, Two-phase mixture numerical simulation of natural convection of nanofluid flow in a cavity partially filled with porous media to enhance heat transfer, *Journal of Molecular Liquids* 238, 2017, 553-569.
- [31] R.Y. Emami, M. Siavashi, G.S. Moghaddam, The effect of inclination angle and hot wall configuration on Cu-water nanofluid natural convection inside a porous square cavity, *Advanced Powder Technology* 29, 2018, 519-536
- [32] S. Mondal, A.S. Dogonchi, N. Tripathi, M. Waqas, S.M. Seyyedi, M. Hashemi-Tilehnoee, D. D. Ganji, A theoretical nanofluid analysis exhibiting hydromagnetics characteristics employing CVFEM, *Journal of the Brazilian Society of Mechanical Sciences and Engineering* (2020), 42:19. <https://doi.org/10.1007/s40430-019-2103-2>
- [33] M. Hashemi-Tilehnoee, A.S. Dogonchi, S.M. Seyyedi, A.J. Chamkha, D.D. Ganji, Magnetohydrodynamic natural convection and entropy generation analyses inside a nanofluid-filled incinerator-shaped porous cavity with wavy heater block, *Journal of*

Thermal Analysis and Calorimetry (2020) <https://doi.org/10.1007/s10973-019-09220-6>

- [34] F. Guerrero Martinez, N. Karimi, Eduardo Ramos, 2018 “Numerical modeling of multiple steady-state convective modes in tilted porous medium heated from below”, *International Communications in Heat and Mass Transfer*, 92, 64-72. <https://doi.org/10.1016/j.icheatmasstransfer.2018.02.009>
- [35] U.S. Choi, J.A. Eastman, Enhancing thermal conductivity of fluids with nanoparticles, *ASME Fed.* 231 (1995) 99–103.
- [36] M. Gupta, V. Singh, R. Kumar, Z. Said, A review on thermophysical properties of nanofluids and heat transfer applications, *Renew. Sustain. Energy Rev.* 74 (2017) 638–670.
- [37] R.A. Mahdi, H.A. Mohammed, K.M. Munisamy, N.H. Saeid, Review of convection heat transfer and fluid flow in porous media with nanofluid, *Renew. Sustain. Energy Rev.* 41 (2015) 715–734.
- [38] A. Kasaeian, R.D. Azarian, O. Mahian, L. Kolsi, A.J. Chamkha, S. Wongwises, I. Pop, Nanofluid flow and heat transfer in porous media: a review of the latest developments, *Int. J. Heat Mass Transf.* 107 (2017) 778–791.
- [39] M. Torabi, C. Dickson, N. Karimi, Theoretical investigation of entropy generation and heat transfer by forced convection of copper-water nanofluid in a porous channel- Local thermal non-equilibrium and partial filling effects, *Powder Technol.* 301 (2016) 234-254. DOI: 10.1016/j.powtec.2016.06.017.
- [40] M.K. Nayak, Sachin Shaw, V.S. Pandey, Ali J Chamkha, Combined effects of slip and convective boundary condition on MHD 3D stretched flow of nanofluid through porous media inspired by non-linear thermal radiation, *Indian J. Phys.*, 92(8) (2018) 1017-1028.
- [41] M. Siavashi, R. Yousofvand, S. Rezanejad, Nanofluid and porous fins effect on natural convection and entropy generation of flow inside a cavity, *Adv. Powder Technol.* 29 (2018) 142–156.
- [42] K. Ghasemi, M. Siavashi, Lattice Boltzmann numerical simulation and entropy generation analysis of natural convection of nanofluid in a porous cavity with different linear temperature distributions on side walls, *J. Molecular Liq.* 233 (2017) 415–430.
- [43] H. Bararnia, Soheli Soleimani, D.D. Ganji, Lattice Boltzmann simulation of natural convection around a horizontal elliptic cylinder inside a square enclosure, *Int. Commun. Heat Mass Transf.* 38 (2011) 1436–1442.

- [44] P. Gholamalipour, M. Siavashi, M. H. Doranehgard, Eccentricity effects of heat source inside a porous annulus on the natural convection heat transfer and entropy generation of Cu-water nanofluid, *Int. Comm. Heat Mass Transf.* 109 (2019) 104367.
- [45] M. Siavashi, S. Mohammad, M. Joibary, Numerical performance analysis of a counter-flow double-pipe heat exchanger with using nanofluid and both sides partly filled with porous media, *J. Therm. Cal.* 135 (2019) 1595-1610.
- [46] S. Asiaei, A. Zadehkafi, M. Siavashi, Multi-layered porous foam effects on heat transfer and entropy generation of nanofluid mixed convection inside a two-sided lid-driven enclosure with internal heating, *Transport in porous media*, 126 (1) (2019) 223-247.
- [47] R. Alizadeh, N. Karimi, A. Mehdizadeh, A. Nourbakhsh, Effect of radiation and magnetic field on mixed convection stagnation-point flow over a cylinder in a porous medium under local thermal non-equilibrium, *Journal of Thermal Analysis and Calorimetry* (2019), DOI: 10.1007/s10973-019-08415-1.
- [48] S. Gomari, R. Alizadeh, A. Alizadeh, N. Karimi, Generation of entropy during forced convection of heat in nanofluid stagnation-point flow over a cylinder embedded in porous media” *Numerical Heat Transfer, Part A: Application*, 75 (2019) 647-673, <https://doi.org/10.1080/10407782.2019.1608774>.
- [49] R. Alizadeh, N. Karimi, R. Arjmandzadeh, A. Mehdizadeh, Mixed convection and thermodynamic irreversibilities in MHD nanofluid stagnation-point flows over a cylinder embedded in porous media, *Journal of Thermal Analysis and Calorimetry* (2018), doi: 10.1007/s10973-018-7071-8.
- [50] A.S. Dogonchi, T. Armaghani, A.J. Chamkha, D.D. Ganji, Natural Convection Analysis in a Cavity with an Inclined Elliptical Heater Subject to Shape Factor of Nanoparticles and Magnetic Field, *Arabian Journal for Science and Engineering* (2019) <https://doi.org/10.1007/s13369-019-03956-x>
- [51] R.L. Hamilton, O.K. Crosser, Thermal conductivity of heterogeneous two component systems, *EC Fundam.* 1 (1962) 187–191.
- [52] R.Ahmad, M.Mustafa, Model and comparative study for rotating flow of nanofluids due to convectively heated exponentially stretching sheet, *Journal of Molecular Liquids* 220, 2016, 635-641
- [53] E.V. Timofeeva, J.L. Routbort, D. Singh, Particle shape effects on thermophysical properties of alumina nanofluids, *Journal of Applied Physics* 106 (2009) 1-11.

- [54] Vaughan R Voller, Basic Control Volume Finite Element Methods for Fluids and Solids (2009) <https://doi.org/10.1142/7027> ISBN: 978-981-283-499-7
- [55] S.M. Seyyedi, A.S. Dogonchi, M. Hashemi-Tilehnoee, M. Waqas, D.D. Ganji, Entropy generation and economic analyses in a nanofluid filled L-shaped enclosure subjected to an oriented magnetic field, *Applied Thermal Engineering* (2019) 114789 <https://doi.org/10.1016/j.applthermaleng.2019.114789>
- [56] A.F. Silva, F.A.S. Marins, E.X. Dias, J.B.S. Oliveira, Modeling the uncertainty in response surface methodology through optimization and Monte Carlo simulation: An application in stamping process, *Materials & Design* 173, 2019, 107776.
- [57] M. Hatami, D. Song, D. Jing, Optimization of a circular-wavy cavity filled by nanofluid under the natural convection heat transfer condition, *International Journal of Heat and Mass Transfer* 98 (2016) 758-767.
- [58] A.H. Pordanjani, S.M. Vahedi, S. Aghakhani, M. Afrand, H.F. Öztop, Effect of magnetic field on mixed convection and entropy generation of hybrid nanofluid in an inclined enclosure: Sensitivity analysis and optimization, *The European Physical Journal Plus* (2019) 134: 412.
- [49] B.S. Kim, D.S. Lee, M.Y. Ha, H.S. Yoon, A numerical study of natural convection in a square enclosure with a circular cylinder at different vertical locations, *International Journal of Heat and Mass Transfer* 51 (2008) 1888-1906.

Table 1: Values of shape factor for diverse nanoparticle shapes [32, 53]

Particle Shapes	Spherical	Cylinder	Platelet
m	3	4.8	5.7

Table 2: Thermo-physical features of H₂O and Cu [41]

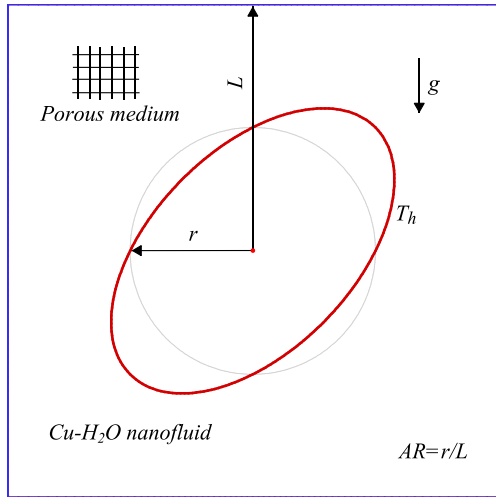
	ρ (kg / m ³)	C_p (J / kg K)	k (W / m K)
Cu	8933	385	401
H ₂ O	997.1	4179	0.6

Table 3: Influence of grid size on Nu_{avg} for $Ra=10^5$, $Da=200$, and $AR=0.5$.

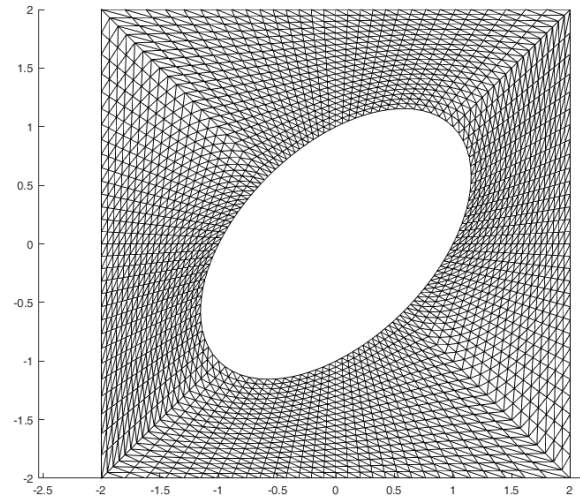
Grid dimension	Nu_{avg}
31×141	2.8677
41×211	2.8253
51×261	2.7652
61×361	2.7630

Table 4: Influence of m on Nu_{avg} for $Da=100$.

Ra	m	$Nu_{ave.}$
10^3	3	0.745366
	4.8	0.767717
	5.7	0.778838
10^4	3	1.315095
	4.8	1.344163
	5.7	1.358467
10^5	3	2.621575
	4.8	2.682951
	5.7	2.713270

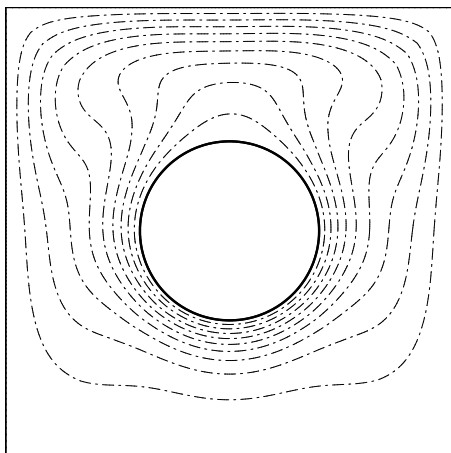


(a)

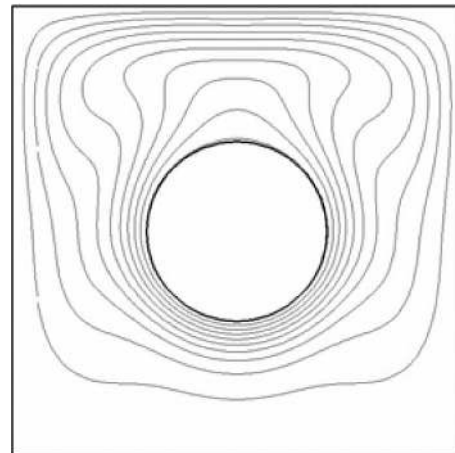


(b)

Fig. 1. (a) Physical model and coordinate system (b) grid distribution



a) Current work



b) Kim et al. [49]

Fig. 2. Comparison between the a) current work and b) Kim et al. [49] at $Ra=10^5$

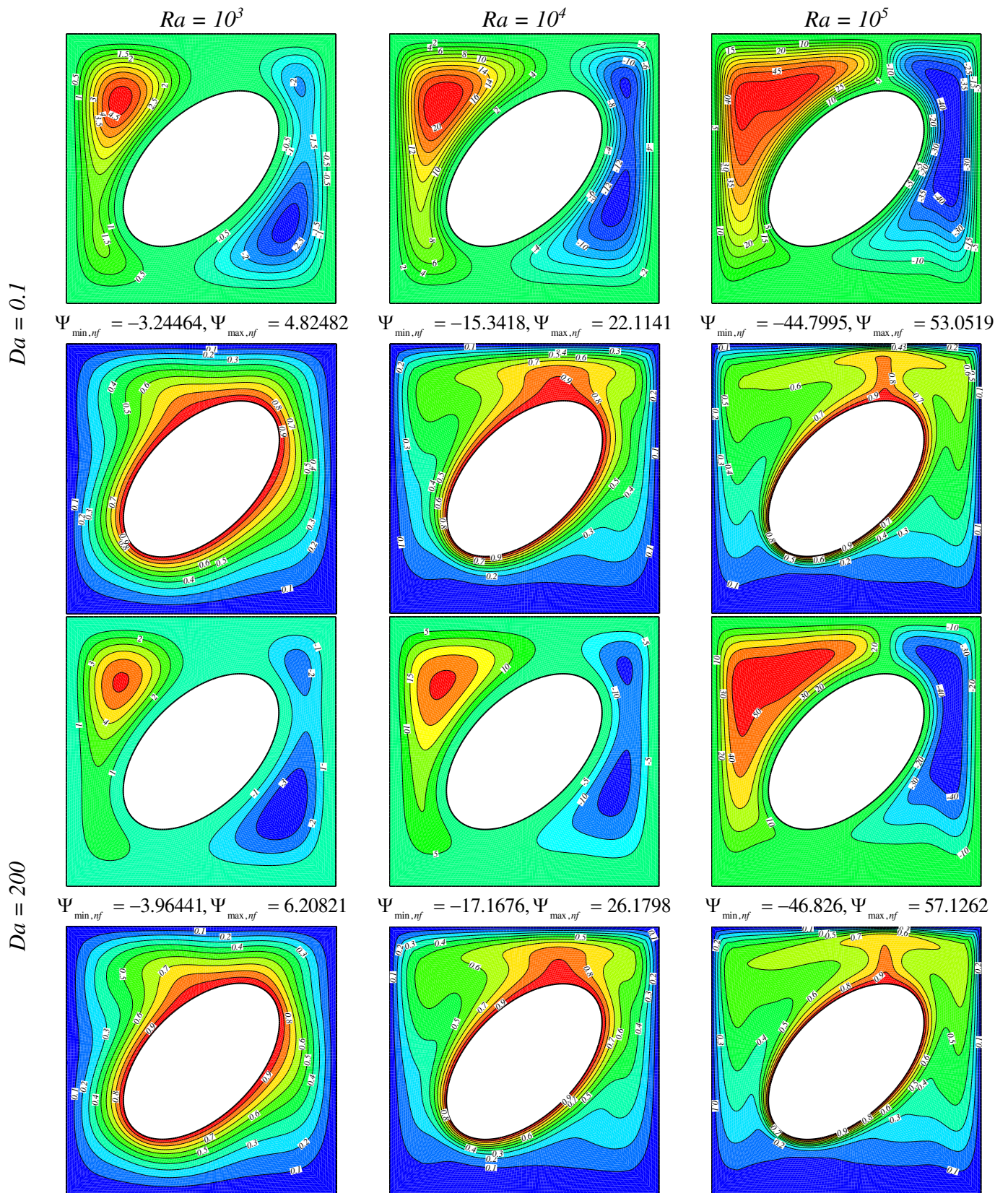


Fig. 3. Streamlines and isotherms for different values of Ra and Da when $\phi = 2\%$, $m=3$ and $AR=0.5$

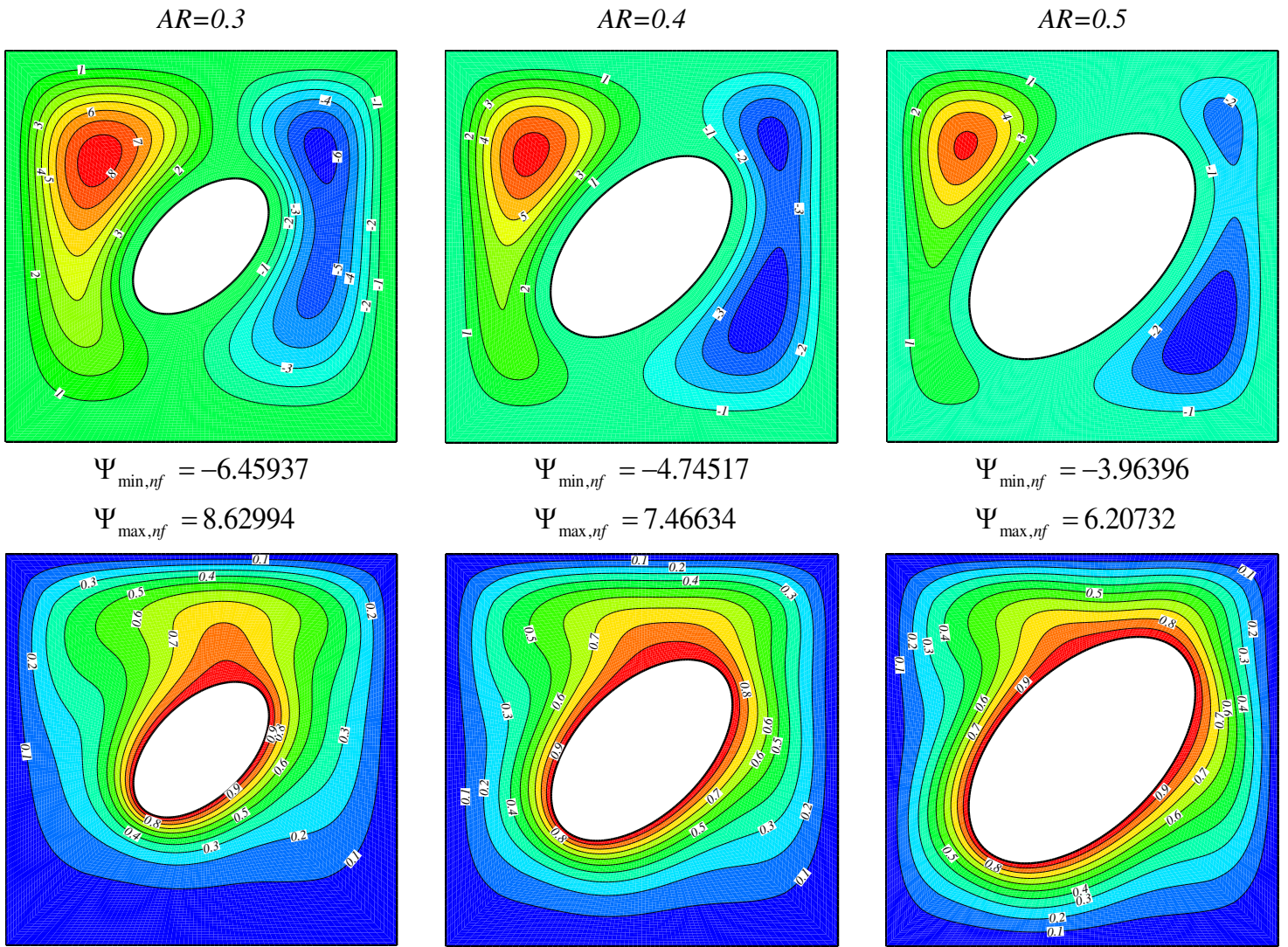


Fig. 4. Streamlines and isotherms for different values of AR when $Ra=10^3$, $Da=100$, $\phi=2\%$ and $m=3$.

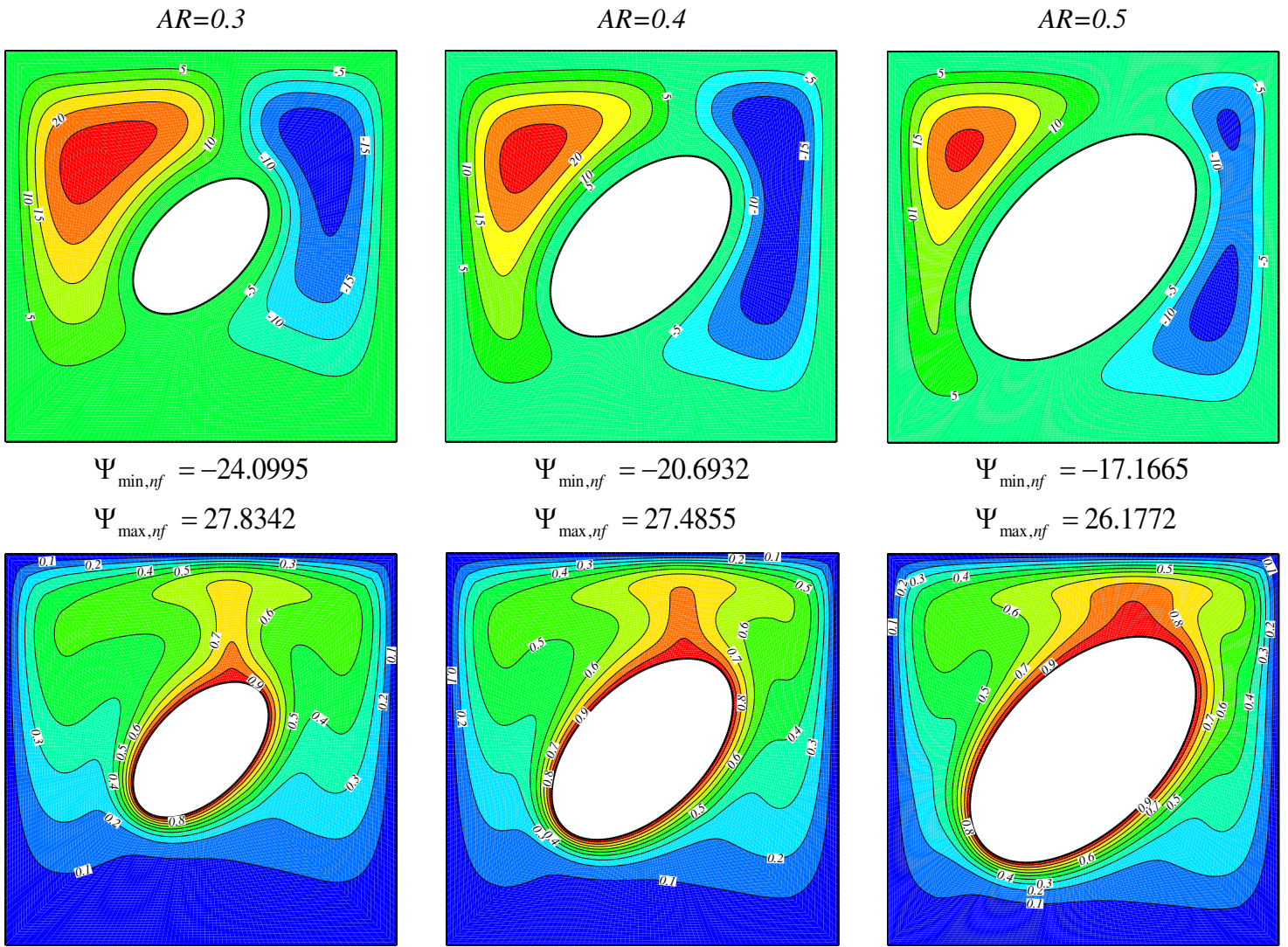


Fig. 5. Streamlines and isotherms for different values of AR when $Ra=10^4$, $Da=100$, $\phi = 2\%$ and $m=3$.

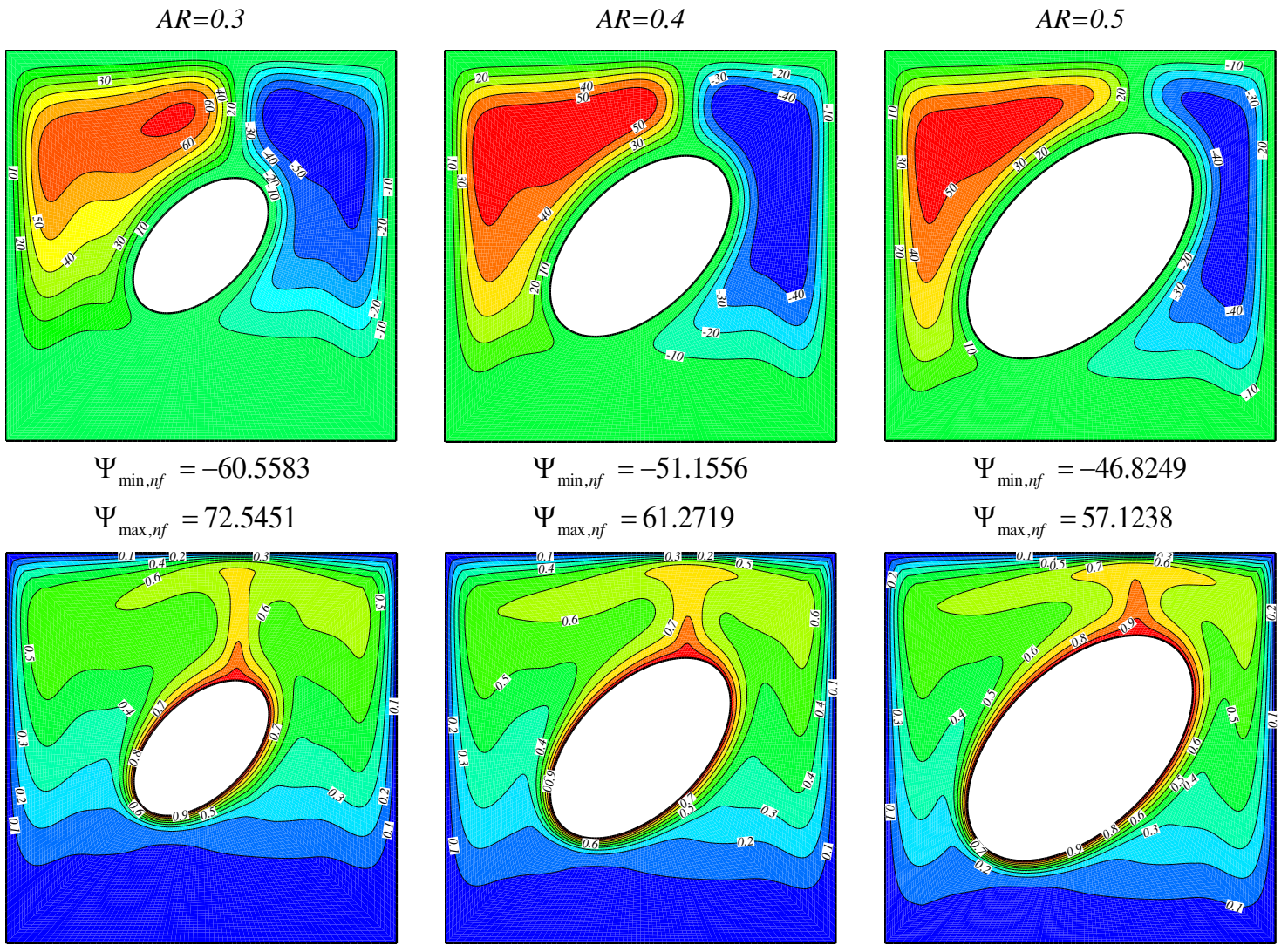


Fig. 6. Streamlines and isotherms for different values of AR when $Ra=10^5$, $Da=100$, $\phi = 2\%$ and $m=3$.

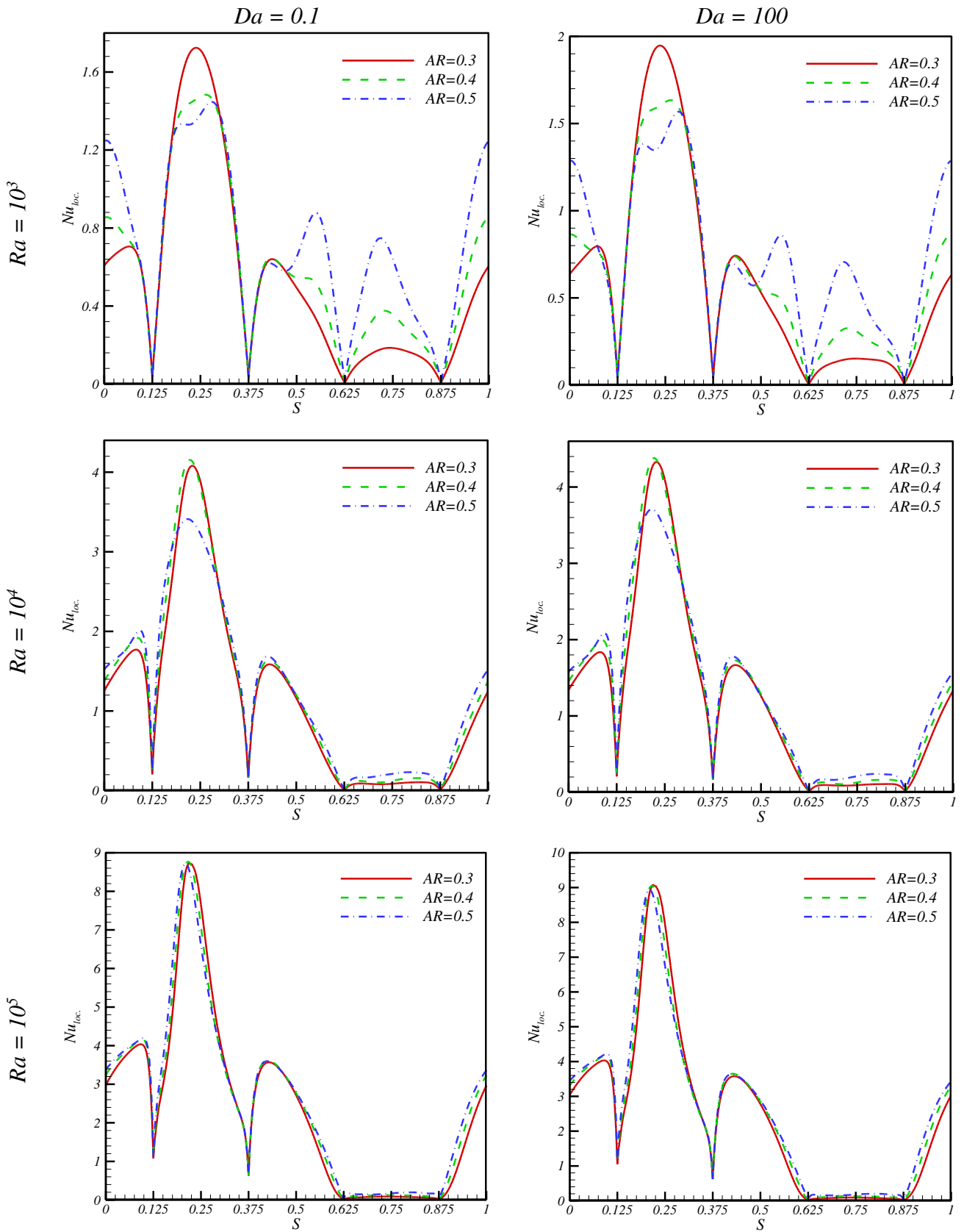


Fig. 7. Local Nusselt number (Nu_{loc}) for different values of Ra , Da and AR when $\phi = 2\%$ and $m=3$

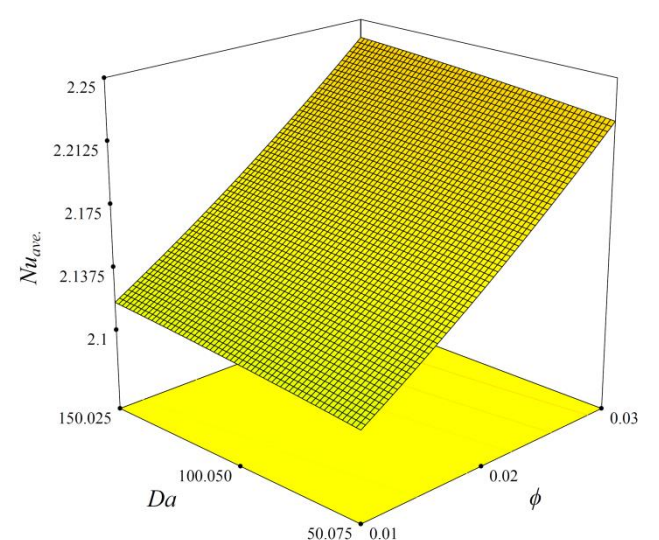
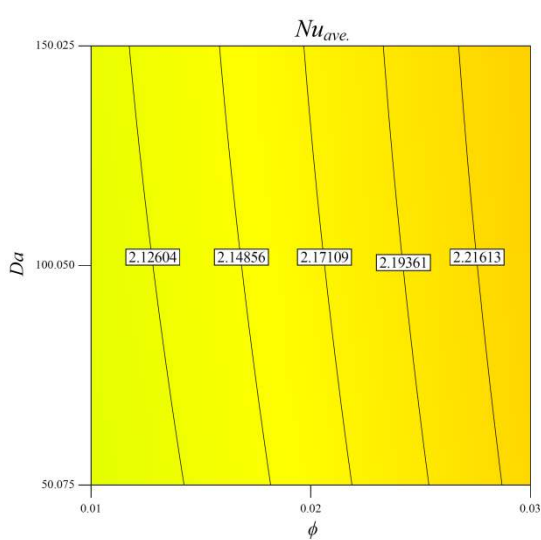
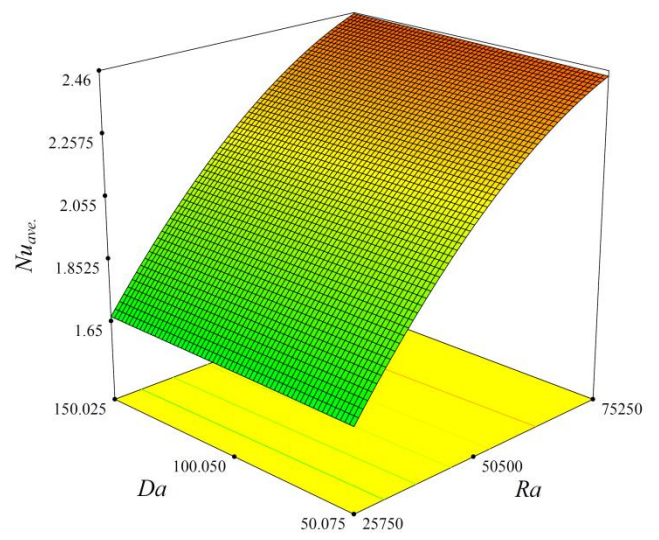
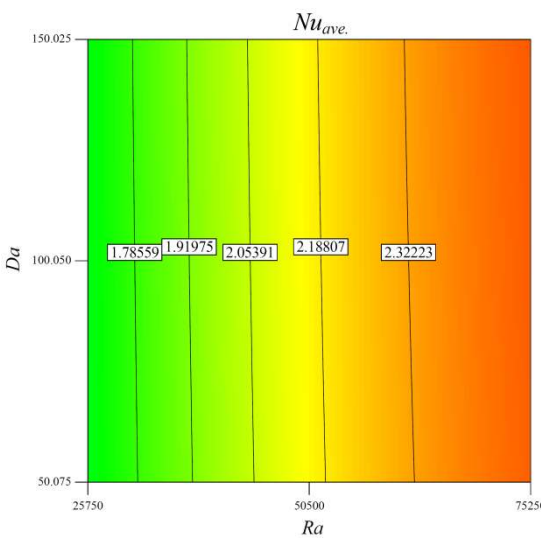
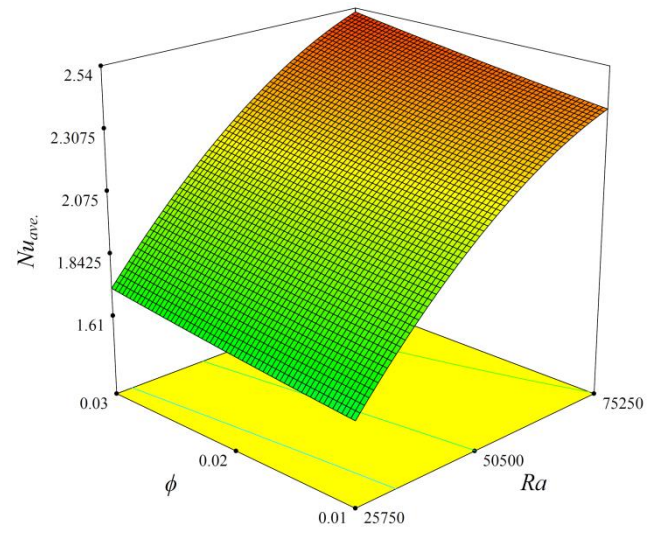
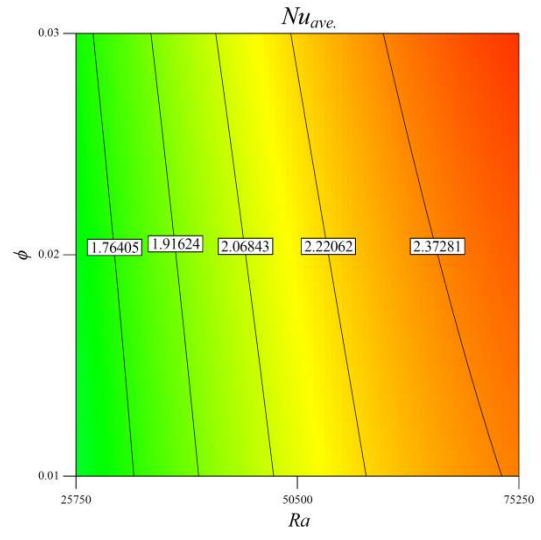


Fig. 8. Average Nusselt number ($Nu_{ave.}$) for different values of Ra , Da and ϕ when $AR=0.5$ and $m=3$.

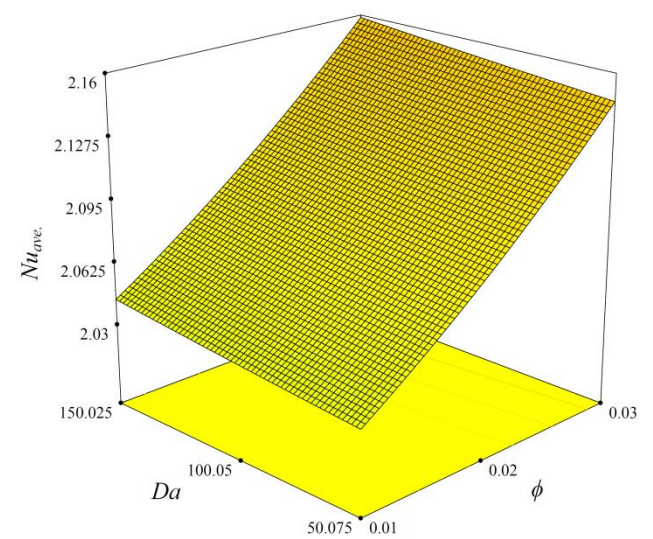
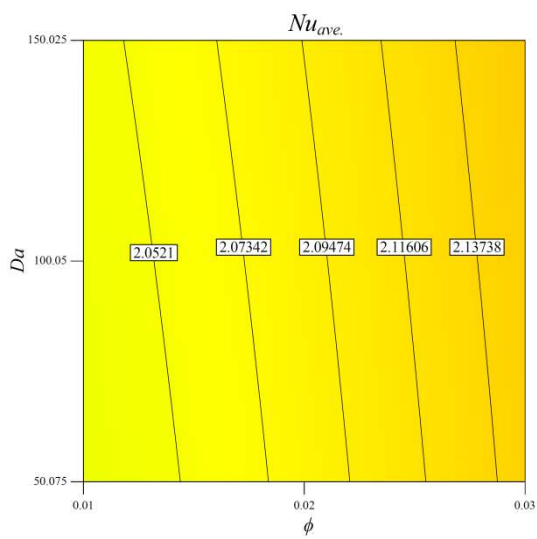
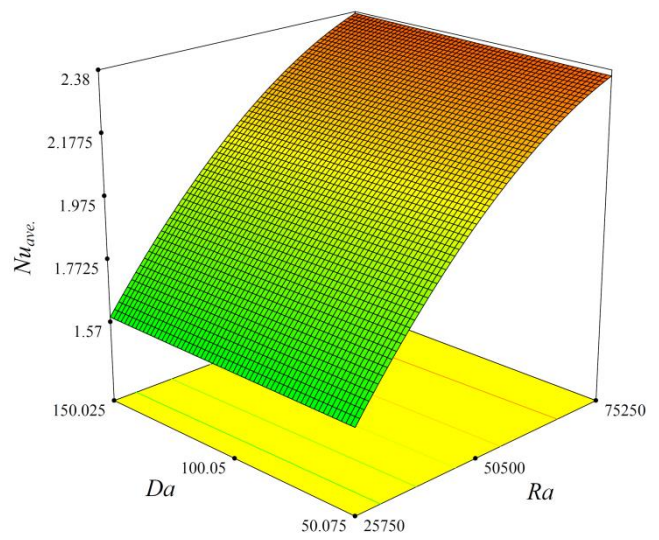
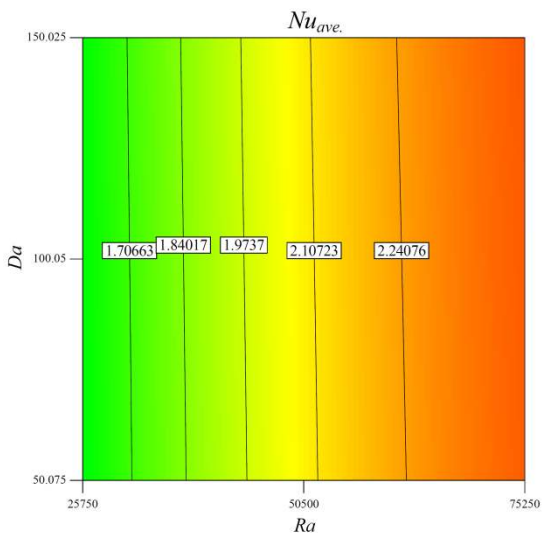
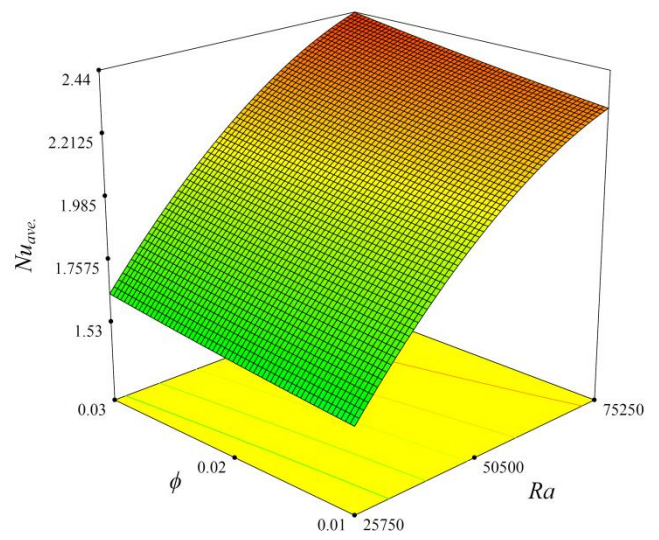
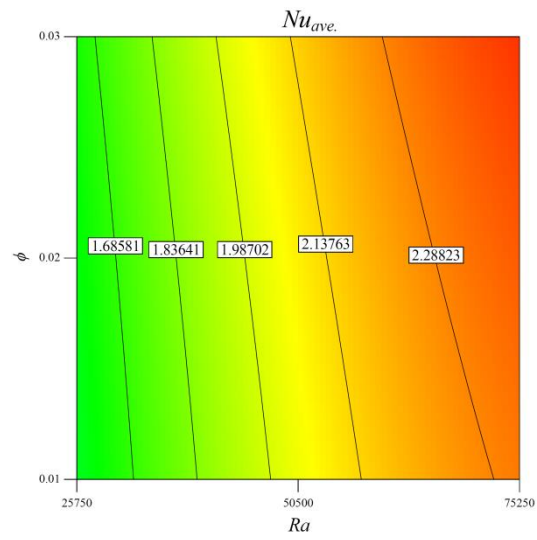


Fig. 9. Average Nusselt number ($Nu_{ave.}$) for different values of Ra , Da and ϕ when $AR=0.4$ and $m=3$.

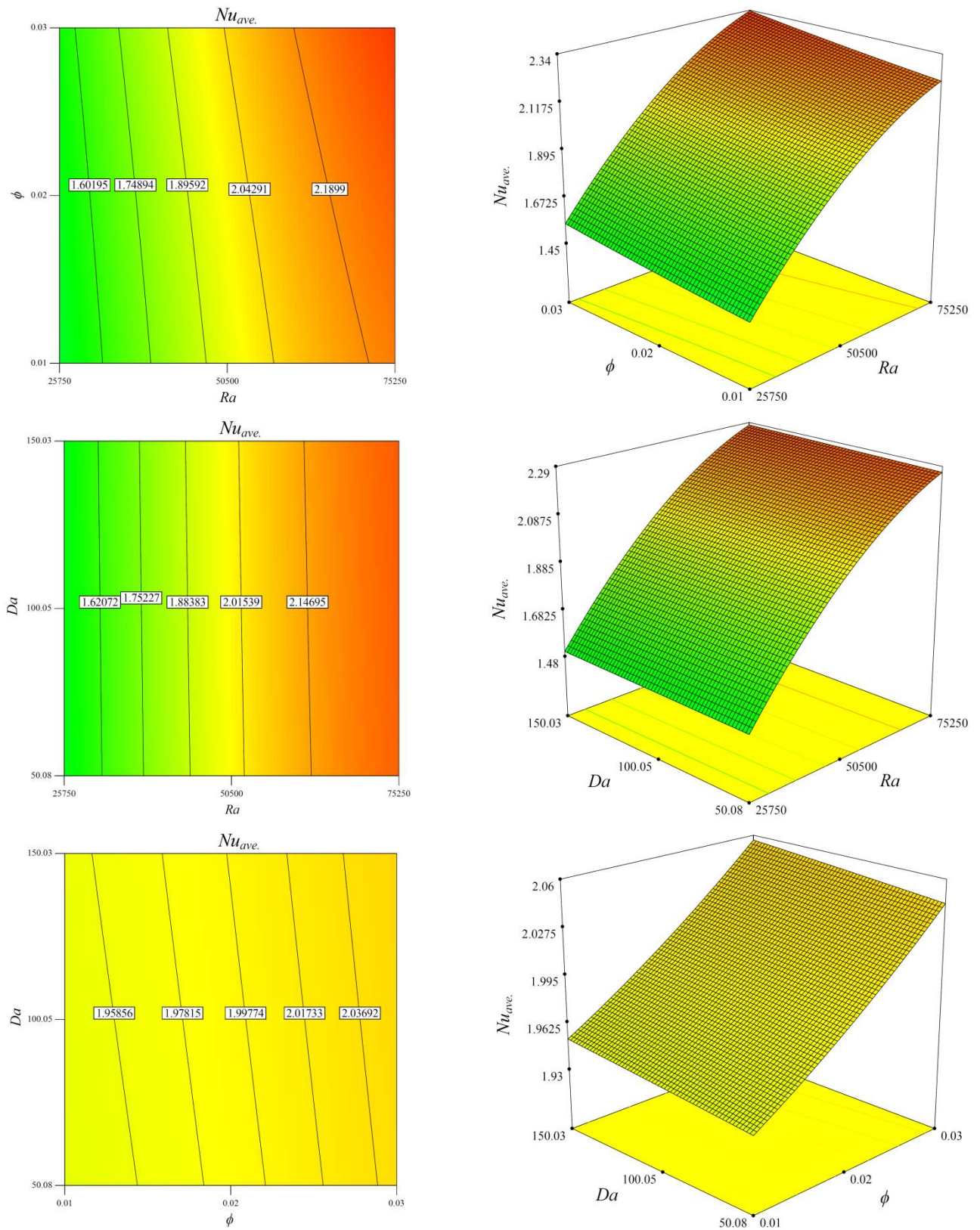


Fig. 10. Average Nusselt number (Nu_{ave}) for different values of Ra , Da and ϕ when $AR=0.3$ and $m=3$.

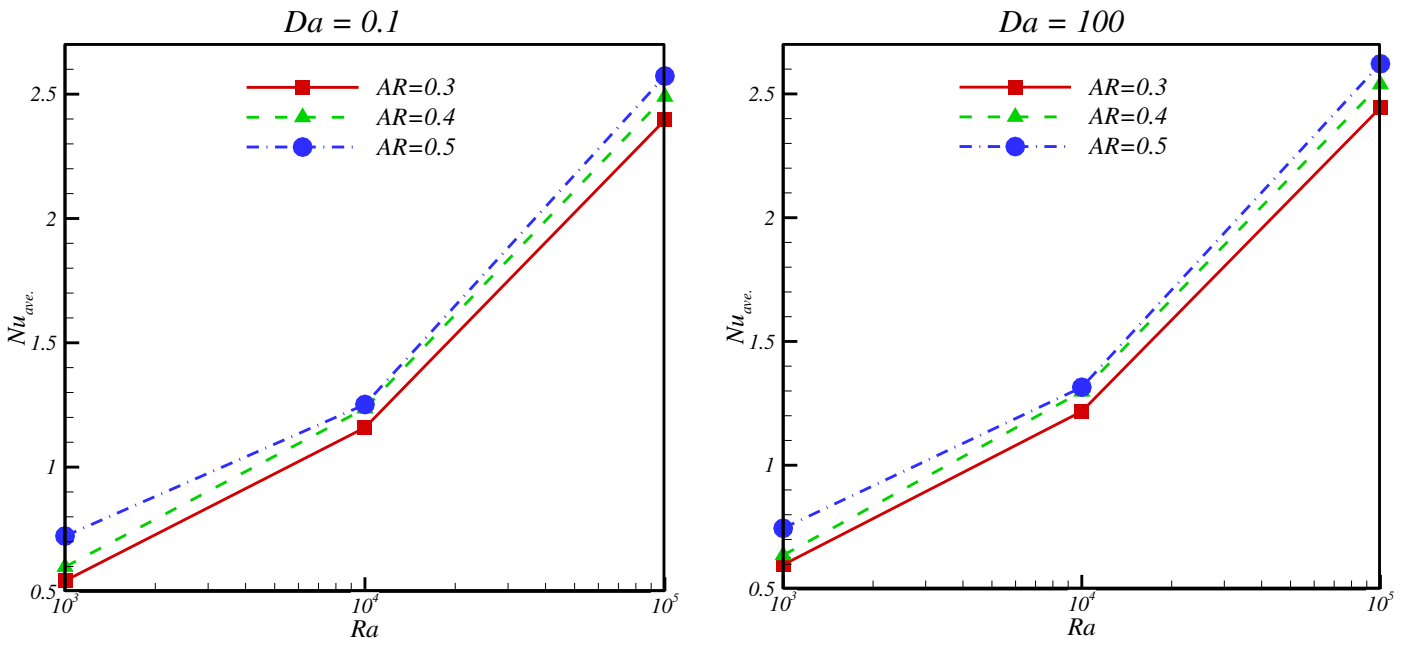


Fig. 11. Average Nusselt number (Nu_{ave}) for different values of AR when $m=3$ and $\phi = 2\%$.